31st Symposium on Naval Hydrodynamics
California, USA, September 11-16, 2016

Comparative study of RANS and LES in simulating cavitating flows

Aswin Gnanaskandan and Krishnan Mahesh
(University of Minnesota, USA)

ABSTRACT

Cavitation refers to formation of vapor when pressure in a liquid drops below vapor pressure of the liquid. This phenomenon is often detrimental and causes noise, vibration and surface erosion. Cavitation is highly unsteady in that the vapor cavities of different sizes form and collapse at different rates, and accurate prediction of this phenomenon is hence imperative. RANS has been the commonly adopted approach to simulate cavitating flows; however LES does a better job in capturing the unsteady dynamics of a cavitating flow. The aim of this paper is to perform a comparative study of RANS and LES in simulating cavitating flows using the same physical model and numerical method. Two different flow configurations are considered each presenting a different challenge and the performance of both RANS and LES is assessed. We consider two-dimensional quasi-steady partial cavitation over a hydrofoil and unsteady sheet to cloud cavitation over a wedge. Numerical results obtained from RANS and LES are compared to each other and with available experimental results.

INTRODUCTION

Cavitation refers to the phenomenon of formation and growth of vapor bubbles when pressure in a liquid drops below vapor pressure. It adversely affects the performance of hydraulic machinery such as pumps, valves and propulsor blades. The formation of vapor is often followed by a growth of the vapor cavity and its violent collapse under high pressure. The physical consequences of this collapse include noise, vibration and surface erosion. A cavitating flow contains a wide range of length and time scales. Vapor cavities of various sizes can form and collapse at different rates which makes their prediction very challenging.

Modeling turbulence in cavitating flows is quite challenging. Steady–state RANS has traditionally been the simplest turbulence model and has been used to predict steady state quantities like cavity length and pressure. Unsteady RANS (URANS) has been successfully used in predicting some quantities in unsteady cavitation. For example, URANS predicts cloud shedding frequency in sheet to cloud cavitation transition to a reasonable accuracy. However, even URANS does not predict all unsteady quantities and LES can potentially be used as a predictive tool in unsteady cavitation problems (Mahesh et al. (2015)).

A number of studies using the homogeneous mixture assumption to study cavitation over two–dimensional geometries (e.g. Singhal et al. (2002); Coutier-Delgosha et al. (2007); Seo and Lele (2009); Goncalves and Patella (2009); Kim (2009)), and three-dimensional geometries with variation in the span and sidewalls (e.g. Saito et al. (2007); Schnerr et al. (2008); Koop and Hoeijmakers (2009); Ji et al. (2013)) have used unsteady RANS to model the turbulence. However, most RANS models need an ad–hoc suppression of eddy viscosity at the cavity interface in order to predict sheet to cloud cavitation (see e.g. Coutier-Delgosha et al. (2007)). Hence LES has been considered by a few authors since it can predict flow unsteadiness better without ad–hoc modifications (e.g. Bensow and Bark (2010); Dittakavi et al. (2010); Ji et al. (2015); Gnanaskandan and Mahesh (2015)). Recently Gnanaskandan and Mahesh (2016a) demonstrated that their LES calculations were able to reproduce sheet to cloud cavitation dynamics over a wedge without any ad–hoc modifications to the turbulence model. In this paper we perform a detailed comparative study of URANS and LES using two different cavitation problems: a quasi steady sheet cavitation over a hydrofoil and an unsteady sheet to cloud cavitation over a wedge.

The paper is organized in the following manner. We first present the 'Governing equation and numerical method' where the physical model, LES and RANS equations and the simulation algorithm are

described. In the section 'Partial cavitation over a hydrofoil', the performance of URANS and LES in a quasi–steady cavitation problem is discussed. Next we discuss 'Sheet to cloud cavitation transition over a wedge', where both LES and URANS results are discussed in detail. The paper is then concluded with a 'Summary' section.

GOVERNING EQUATIONS AND NUMERICAL METHOD

We use the homogeneous mixture model that assumes the mixture of constituent phases to be a single compressible fluid. Surface tension effects are assumed small and are neglected. The governing equations are the compressible Navier Stokes equation for the mixture of liquid and vapor along with a transport equation for vapor. The density of the homogeneous mixture is given by

$$\rho = \rho_l(1-\alpha) + \rho_g\alpha, \tag{1}$$

where ρ_l is the density of liquid and ρ_g is the density of vapor. α is the vapor volume fraction which is related to the vapor mass fraction (Y) by

$$\rho_l(1-\alpha) = \rho(1-Y) \quad \text{and} \quad \rho_g\alpha = \rho Y. \tag{2}$$

The transport equation for mass fraction of vapor is given by

$$\frac{\partial \rho Y}{\partial t} = -\frac{\partial}{\partial x_k}\left(\rho Y u_k\right) + S_e - S_c,$$

Here, S_e and S_c are the source terms for evaporation of water and condensation of vapor and are given by

$$\begin{aligned} S_e &= C_e\alpha^2(1-\alpha)^2\frac{\rho_l}{\rho_g}\frac{\max(p_v-p,0)}{\sqrt{2\pi R_g T}}, \\ S_c &= C_c\alpha^2(1-\alpha)^2\frac{\max(p-p_v,0)}{\sqrt{2\pi R_g T}}, \end{aligned} \tag{3}$$

where p_v is the vapor pressure. C_e and C_c are empirical constants whose value is 0.1 (Saito et al., 2007). The system is closed using a mixture equation of state given by

$$p = Y\rho R_g T + (1-Y)\rho K_l T\frac{p}{p+P_c}. \tag{4}$$

The values of all the constants in the equation of state are given in Gnanaskandan and Mahesh (2015).

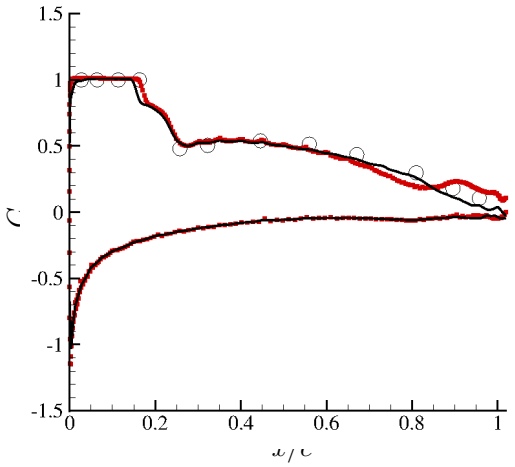

Figure 1: Comparison of pressure co-efficient (C_p) distribution, ∘ : Shen and Dimotakis (1989), □ : URANS, ——— : LES.

LES

To perform LES, the governing equations are first Favre filtered spatially:

$$\begin{aligned} \frac{\partial \overline{\rho}}{\partial t} &= -\frac{\partial}{\partial x_k}\left(\overline{\rho}\tilde{u_k}\right), \\ \frac{\partial \overline{\rho}\tilde{u_i}}{\partial t} &= -\frac{\partial}{\partial x_k}\left(\overline{\rho}\tilde{u_i}\tilde{u_k} + \overline{p}\delta_{ik} - \tilde{\sigma}_{ik} - \tau_{ik}\right), \\ \frac{\partial \overline{\rho}\tilde{Y}}{\partial t} &= -\frac{\partial}{\partial x_k}\left(\overline{\rho}\tilde{Y}\tilde{u_k} - t_k\right) + \tilde{S}_e - \tilde{S}_c, \\ \frac{\partial \overline{\rho}\tilde{e}_s}{\partial t} &= -\frac{\partial}{\partial x_k}\left(\overline{\rho}\tilde{e_s}\tilde{u_k} - \tilde{Q}_k - q_k\right) - \overline{p}\frac{\partial \tilde{u_k}}{\partial x_k} + \tilde{\sigma_{ik}}\frac{\partial \tilde{u_i}}{\partial x_k}. \end{aligned}$$

Here, the tilde quantities are Favre averaged quantities and τ_{ik}, q_k and t_k are subgrid scale (SGS) terms namely: SGS stress, SGS heat flux and SGS scalar flux. These terms are modeled using the Dynamic Smagorinsky model (DSM) :

$$\begin{aligned} \tau_{ij} - \frac{\delta_{ij}}{3}\tau_{kk} &= -2C_S(\mathbf{x},t)\overline{\rho}\Delta^2\left|\tilde{S}\right|\widetilde{S^*_{ij}}, \\ \tau_{kk} &= 2C_I(\mathbf{x},t)\overline{\rho}\Delta^2\left|\tilde{S}\right|^2, \\ q_i &= -\overline{\rho}\frac{C_S(\mathbf{x},t)\Delta^2\left|\tilde{S}\right|}{Pr_T}\frac{\partial \overline{T}}{\partial x_i}, \\ t_i &= -\overline{\rho}\frac{C_S(\mathbf{x},t)\Delta^2\left|\tilde{S}\right|}{Sc_T}\frac{\partial \overline{Y}}{\partial x_i}, \end{aligned} \tag{5}$$

where $|S| = \sqrt{2S_{ij}S_{ij}}$ and $S^*_{ij} = S_{ij} - 1/3S_{kk}\delta_{ij}$. The model coefficients C_s, C_I, Pr_T and Sc_T are de-

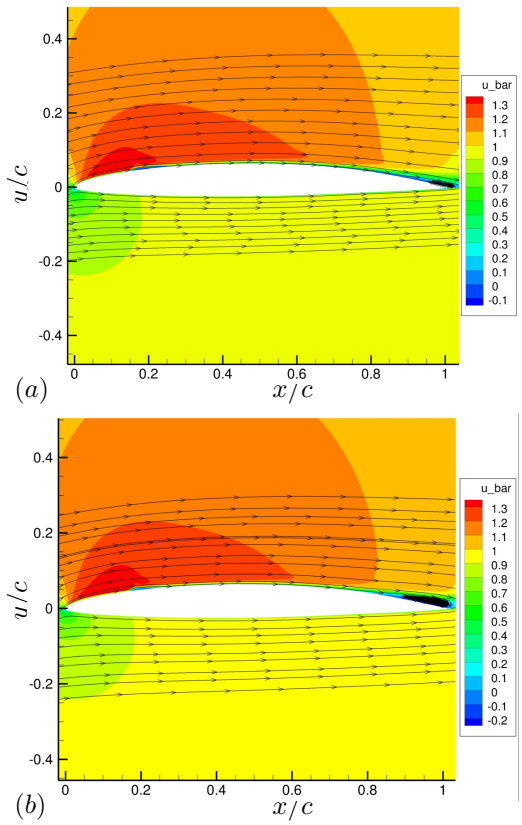

Figure 2: Mean streamwise velocity contours for (a) LES and (b) URANS.

termined using the Germano identity. For example,

$$\begin{aligned} C_S\Delta^2 &= \frac{1}{2}\frac{\langle L_{ij}^* M_{ij}^* \rangle}{\langle M_{ij}^* M_{ij}^* \rangle}, \\ L_{ij}^* &= \left(\frac{\widehat{\overline{\rho u_i}\cdot\overline{\rho u_j}}}{\overline{\rho}}\right) - \frac{\widehat{\overline{\rho u_i}}\cdot\widehat{\overline{\rho u_j}}}{\widehat{\overline{\rho}}}, \\ M_{ij}^* &= \overline{\rho}\widehat{\left|\tilde{S}\right|\widetilde{S_{ij}^*}} - \widehat{\overline{\rho}}\left(\frac{\widehat{\Delta}}{\Delta}\right)^2 \widehat{\left|\tilde{S}\right|}\widehat{\widetilde{S_{ij}^*}}, \end{aligned} \tag{6}$$

where, $\langle\cdot\rangle$ denotes spatial average over neighboring control volumes and the caret denotes test filtering. Test filtering is defined by the linear interpolation from face values of a control volume, which is again the interpolation from two adjacent cell center values (Park and Mahesh, 2007):

$$\widehat{\phi} = \frac{1}{N_{\text{face}}}\sum_{\text{no of face}}\phi_f = \frac{1}{2N_{\text{face}}}\sum_{\text{no of face}}(\phi_{icv1}+\phi_{icv2}), \tag{7}$$

where N_{face} is the number of faces for a given control volume.

URANS

For unsteady RANS, the Spalart-Allmaras model Spalart and Allmaras (1992) is used:

$$\begin{aligned} &\frac{\partial\rho\tilde{\nu}}{\partial t} + \frac{\partial(\rho\tilde{\nu}u_k)}{\partial x_k} = c_{b1}\tilde{S}\rho\tilde{\nu} + \\ &\frac{1}{\sigma}\left[(1+c_{b2})\nabla\cdot\left((\rho\nu+\rho\tilde{\nu})\nabla\tilde{\nu}\right) - c_{b2}\left(\rho\nu+\rho\tilde{\nu}\right)\nabla\cdot\nabla\tilde{\nu}\right] \\ &\qquad - \rho c_{w1} f_w \left(\frac{\tilde{\nu}}{d}\right)^2. \end{aligned} \tag{8}$$

where $\nu_T = \tilde{\nu} f_{v1}$, $f_{v1} = \chi^3/(\chi^3 + c_{v1})$ and $\chi = \tilde{\nu}/\nu$. S is the strain rate. The model is closed with the following coefficients and wall functions:

$$\begin{aligned} &\tilde{S} = S + \tfrac{\tilde{\nu}}{\kappa^2 d^2} f_{v2},\ f_{v2} = \left(1 + \tfrac{\chi}{c_{v2}}\right)^{-3}, \\ &f_w = g\left(\tfrac{1+c_{w3}^6}{g^6+c_{w3}^6}\right)^{1/6},\ g = r + c_{w2}(r^6 - r),\ r = \tfrac{\tilde{\nu}}{\tilde{S}\kappa^2 d^2}, \\ &c_{b1} = 0.1355,\ \sigma = \tfrac{2}{3},\ c_{b2} = 0.622,\ \kappa = 0.41,\ c_{v2} = 5, \\ &c_{w1} = \tfrac{c_{b1}}{\kappa^2} + \tfrac{1+c_{b2}}{\sigma},\ c_{w2} = 0.3,\ c_{w3} = 2,\ c_{v1} = 7.1. \end{aligned} \tag{9}$$

For cavitating flows, Coutier-Delgosha et al. (2003) observed that the eddy viscosity obtained from standard RANS models can be excessive, especially near the cavity closure region, which prevents cloud formation. Hence they suggested to modify the eddy viscosity near the cavity interface as

$$\mu_T = \nu_T[\rho_g + (\rho_l - \rho_g)(1-\alpha)^{10}]. \tag{10}$$

Once ν_T is computed, the Reynolds stress is given by

$$\mathcal{R}_{ij} = -2\rho\nu_T\overline{S}_{ij}. \tag{11}$$

The turbulent thermal conductivity and turbulent scalar diffusivity are also computed from the eddy viscosity assuming a turbulent Prandtl number (Pr_t) of 0.9 and a turbulent Schmidt number (Sc_t) of 0.7. The turbulent scalar equation is then modified as

$$\frac{\partial\rho Y}{\partial t} = -\frac{\partial}{\partial x_k}(\rho Y u_k) + S_e - S_c + \frac{\partial}{\partial x_k}\left(\frac{\nu_t}{Sc_t}\frac{\partial\rho Y}{\partial x_k}\right). \tag{12}$$

The simulation algorithm is described in detail elsewhere (Gnanaskandan and Mahesh (2015)). The algorithm has been validated for a variety of flows including a cavitating shock tube, turbulent cavitating flow over a hydrofoil Gnanaskandan and Mahesh (2014, 2015) and a hemispherical headform Gnanaskandan and Mahesh (2016b).

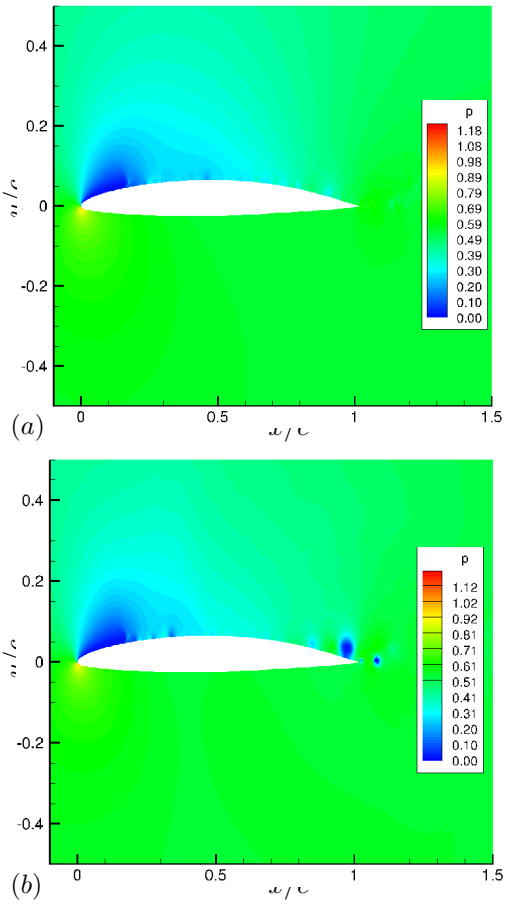

Figure 3: Instantaneous pressure contours, (a) : LES and (b) : URANS.

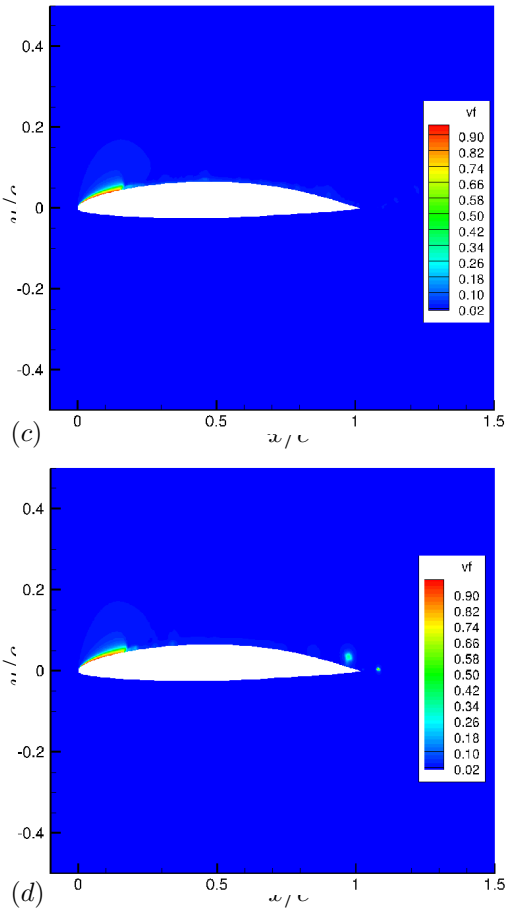

Figure 4: Instantaneous void fraction contours, (a) : LES and (b) : URANS.

PARTIAL CAVITATION OVER A HYDROFOIL

We consider a turbulent cavitating flow over a hydrofoil. Shen and Dimotakis (1989) conducted experiments on this hydrofoil and our numerical results are compared against their experimental results. The hydrofoil section used is NACA 66 (mod) with a camber ratio of 0.02 and a thickness ratio of 0.09. The Reynolds number based on chord length c is 2 $\times 10^6$, the angle of attack is 4 degrees and the cavitation number $\sigma = \frac{p_\infty - p_v}{0.5\rho_\infty u_\infty^2}$ is 1.0. At this cavitation number, a leading edge cavity, also referred as partial sheet cavity/open cavity (Leroux et al., 2004; Laberteaux and Ceccio, 2001) is observed in the experiment. A streamwise grid spacing of 0.0005c is used near the stagnation region to capture cavitation inception and the wall normal spacing is 0.0008c. The three–dimensional grid for LES has 75 cells in the span–wise direction. We perform both LES and RANS and the results are compared to the experimental results.

Figure 1 shows the time averaged pressure coefficient distribution along the chord for both the suction and pressure sides. Both LES and RANS give reasonable agreement; the LES result however shows better agreement near the trailing edge when compared to RANS. This difference between RANS and LES can be understood from Figure 2 showing mean streamwise velocity contour. RANS predicts a larger separation bubble in the trailing edge when compared to LES and it is this discrepancy that causes the RANS result to deviate from the experimental result near the trailing edge. However, in the cavity region both URANS and LES do an equally good job in predicing both the cavity length and pressure distribution inside the cavity. This comes as no surprise since URANS is expected to perform well in steady and quasi–steady conditions such as this.

The quasi–steady nature of the flow can be understood from instantaneous pressure and void frac-

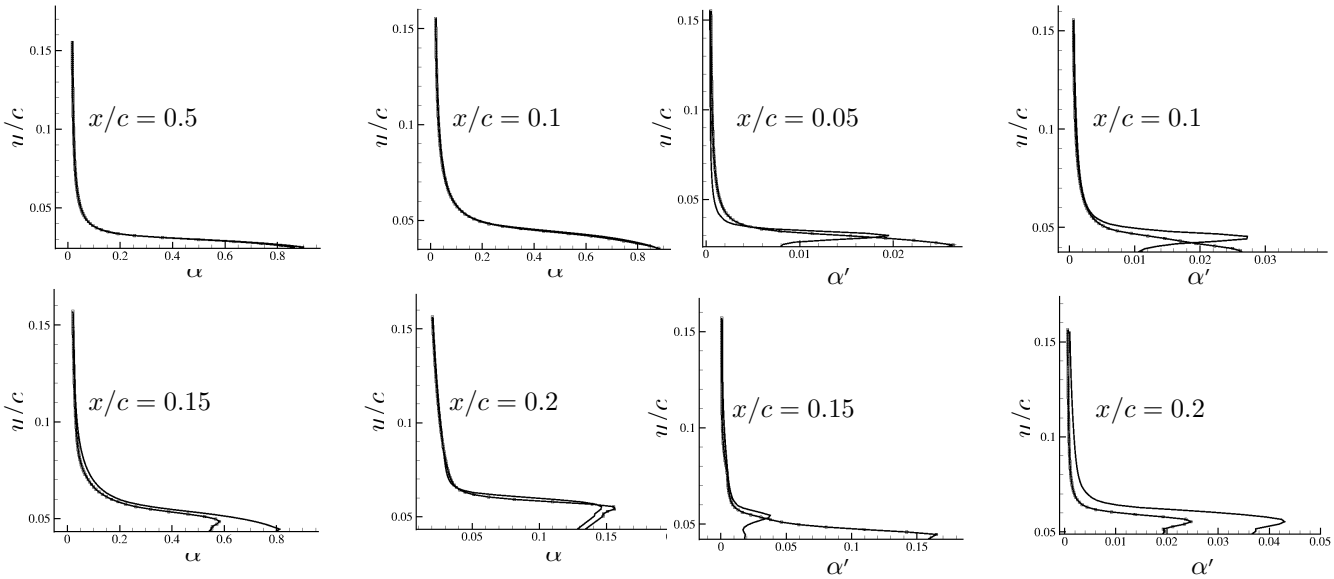

Figure 5: Comparison of mean void fraction from LES and RANS at different streamwise stations, —— : RANS, —— □—— : LES.

Figure 6: Comparison of RMS of void fraction from LES and RANS at different streamwise stations, —— : RANS, —— □—— : LES.

tion contours in Figures 3 and 4. The pressure contours suggest that both LES and URANS predict the shedding phenomenon behind the quasi–steady cavity. However, the vortices shed in URANS are more coherent and two–dimensional in nature. The absence of vortex stretching in two–dimensions leads to more intense vortex having lower pressure levels in the vortex core. The three dimensional effects in LES leads to a more realistic shedding behavior. From the void fraction contours, we can observe that the core of vortices cavitate again near the trailing edge in the URANS case and this behavior is absent in the LES.

Figures 5 and 6 show the mean and RMS void fraction profiles at four different streamwise locations inside the mean cavity. The first station ($x/c = 0.05$) is very close the leading edge near the inception location and the final station($x/c = 0.2$) is at the mean cavity closure. The predictions from URANS and LES are very close to each other except that URANS predicts a larger mean void fraction inside the cavity except near the cavity closure. and LES predicts higher fluctuations than RANS. Note that the RMS contains only the resolved part of the fluctuations.

SHEET TO CLOUD CAVITATION TRANSITION OVER A WEDGE

The performance of URANS and LES in an unsteady cavitation problem is next compared using sheet to cloud transition over a wedge. The simulation corresponds to the experiment of Ganesh (2015), where the height of the wedge is $h = 1$ inch. In order to minimize the effect of acoustic reflection from the boundaries, the computational domain is extended in both upstream ($25h$) and downstream directions ($50h$) , in addition to applying to acoustically absorbing boundary conditions Colonius (2004). Velocity and pressure are prescribed at the inlet and downstream pressure is prescribed at the outlet. No slip boundary conditions are imposed on top and bottom walls. Periodic boundary conditions are enforced at the spanwise boundaries. The Reynolds number of the flow based on the wedge height ($h = 1$ inch) and a bulk velocity of 7.9 m/s is approximately 0.2×10^6 and the cavitation number is 2.1. The mesh is made very fine near the wedge apex and along the entire length of the wedge where the major portion of the vapor is expected to form. The minimum grid spacing near the wedge is $0.001h \times 0.001h$ in the wall normal and streamwise directions respectively. The wall normal spacing stretches to $0.005h$ at a height of $0.5h$ from the wedge apex and further to about $0.01h$ at a height of h from the apex. In the streamwise direction, the

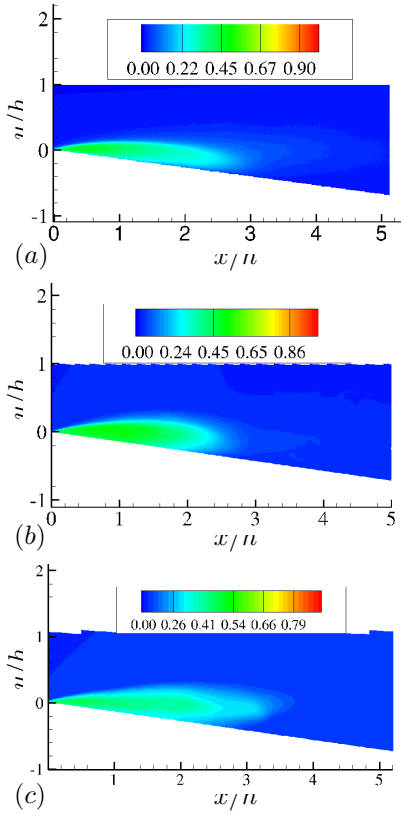

Figure 7: Comparison of mean void fraction contours, (a) Experiment, (b) LES and (c) URANS.

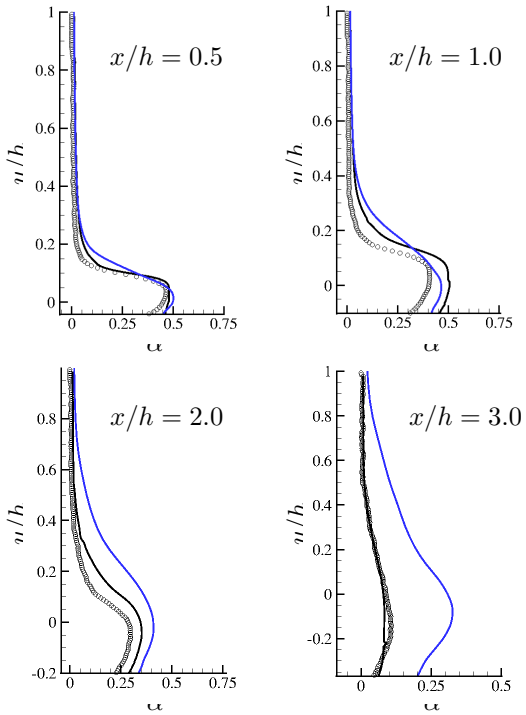

Figure 8: Comparison of mean void fraction profiles at different streamwise locations, ∘ : Experiment (Ganesh (2015)), ——— : LES, ——— : unsteady RANS.

grid is stretched to $0.02h$ at a distance $3.5h$ from the apex and further to $0.01h$ at the end of the wedge. The LES grid has 80 points in the spanwise direction.

The time averaged values in the simulations are obtained by performing time average over four shedding cycles. For the LES simulations, further convergence is obtained by averaging along the statistically homogeneous spanwise direction as well. Figure 7 shows the mean void fraction contours obtained from experiment, LES and URANS. A good agreement is obtained for cavity length and the value of mean void fraction inside the cavity between LES and experiment. The URANS simulation predicts a larger cavity length. The cavity thickness predicted by LES is slightly larger than the experimental measurement while that predicted by URANS is even larger than LES. Thus LES does a better job in predicting the cavity dimensions.

The mean void fraction at different streamwise locations on the wedge obtained from LES and URANS are compared to the experimental results in Figure 8. Note the overall good agreement of the value of mean void fraction inside the cavity for LES in contrast to unsteady RANS. Further, the length of the cavity is also not predicted well by unsteady RANS, while LES gives an excellent agreement for the mean length. The thickness is slightly mispredicted by LES at stations $x/h = 1.0$ and $x/h = 2.0$, while the thickness predicted by unsteady RANS is even worse. Overall, LES agrees much better with the experiments than unsteady RANS. No error bars are available from experiment for mean void fraction data. Next we compare the RMS of void fraction obtained from simulations and experiment in Figure 9. Note that error bars are not available from the experiment for this quantity either, and that only the resolved portion of the fluctuation obtained from LES is shown here. The free stream fluctuation measured in the experiment does not go to zero while that predicted by LES and URANS goes to zero away from the cavity. The qualitative trend from LES agrees well with the experiment at all the stations and LES also seems to predict the RMS much better than unsteady RANS. The fact that LES predicts a thicker cavity is also manifested in the form of higher magnitude of fluctuations away from the wedge. Overall, the comparisons for void fraction data are encouraging suggesting the suitability of LES in predicting

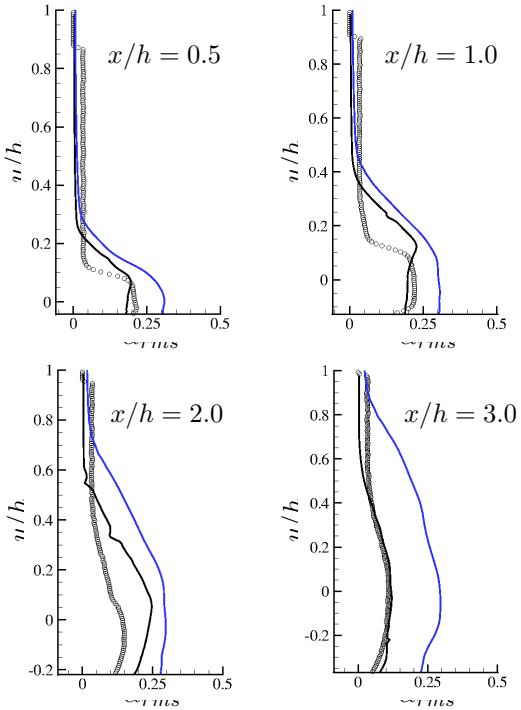

Figure 9: Comparison of RMS of void fraction profiles at different streamwise locations, ∘ : Experiment (Ganesh (2015)), ——— : LES, ——— : unsteady RANS.

this highly unsteady phenomenon.

To compare the local cavitation characteristics, two quantities $\overline{\sigma}_{loc} = 2(\overline{p} - p_v)/\rho_\infty u_\infty^2$ and $\sigma^{'} = 2\sqrt{\overline{p'^2}}/\rho_\infty u_\infty^2$ are defined. Figure 10(a) and (b) show the variation of $\overline{\sigma}_{loc}$ and $\sigma^{'}$ along the wedge. $x/h = 0$ is the apex region and minimum $\overline{\sigma}_{loc}$ is obtained there. It is interesting to see that the mean pressure never falls below the vapor pressure for both LES and RANS, but the fluctuations at the apex are large enough for the instantaneous local pressure to fall below vapor pressure. Note that the value of RMS of pressure is maximum $x/h = 2.5$ which corresponds to the mean closure location of the cavity. This behavior points to cavity oscillation about that position. Interestingly, URANS predicts larger local cavitation number at the inception location, which points to higher mean pressure in that region. However, the pressure fluctuation at the apex predicted by URANS is about three times that predicted by LES. Further URANS consistently predicts higher fluctuation values leading to an increased amount of vapor production. Interestingly the RMS of vapor fraction predicted by URANS is higher than that of LES. Thus there is a consistent trend of all fluctuation quantities being over predicted by URANS.

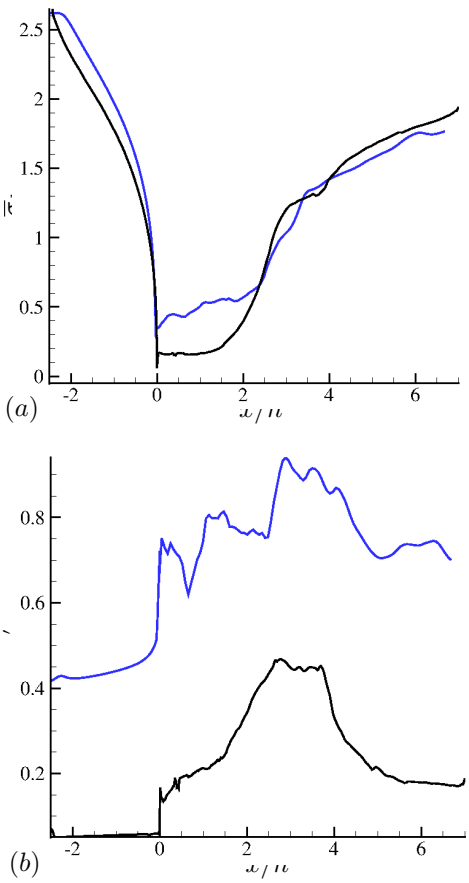

Figure 10: Variation of (a):$\overline{\sigma}_{loc}$ and (b) : σ' along the wedge wall,——— : LES, ——— : unsteady RANS.

Figure 11(b) shows the variation of mean density and mean volume fraction along the wedge. It is clear that inception occurs at the apex and the maximum amount of vapor in the mean flow occurs inside the sheet cavity. The region corresponding to the cloud has lesser void fraction than that in the sheet. This observation is also in line with the observations of Coutier-Delgosha et al. (2007). URANS predicts lesser mean vapor fraction immediately after inception near the wall. However as we move downstream URANS predicts more vapor closer to the wall than LES. Overall, LES agrees better with experiments when compared to URANS.

SUMMARY

A comparative study of URANS and LES has been performed for two different turbulent cavitating problems using the same physical model and nu-

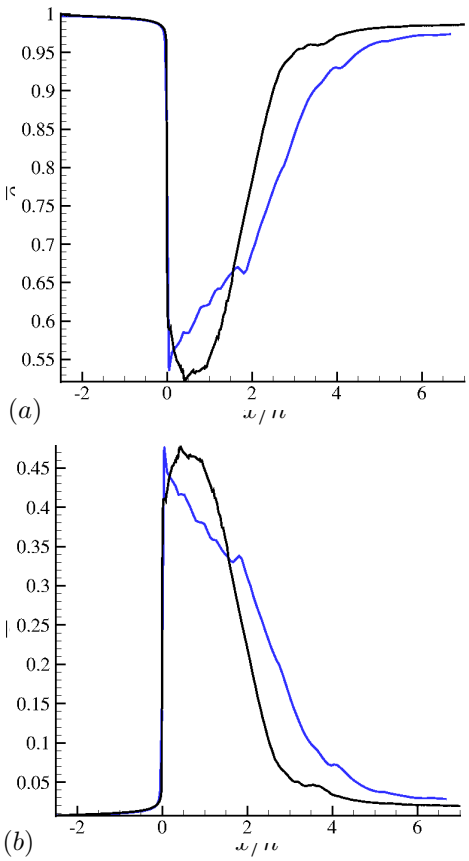

Figure 11: Variation of (a): mean density and (b): mean void fraction along the wedge wall,——— : LES, ——— : unsteady RANS.

merical method. For the quasi–steady partial cavity over a hydrofoil both URANS and LES are able to capture the unsteady shedding vortices behing the quasi–steady cavity. Further, the cavity length, pressure drop inside the cavity and the pressure increase at the closure location are also predicted well by both URANS and LES. It is not surprising that URANS performs well for this case. The comparisons between URANS and LES show a stark contrast in the unsteady sheet to cloud cavitation over a wedge. LES predicts both mean and RMS of void fraction inside the vapor cavity and near the cavity closure to a much better accuracy than URANS. It is also observed that URANS predicts much higher fluctuations for almost all quantities which might explain the discrepancy with the experimental results.

ACKNOWLEDGMENT

This work was supported by the United States Office of Naval Research under ONR Grant N00014-11-1-0497 with Dr. Ki-Han Kim as the program manager. Computing resources were provided by the Arctic Region Supercomputing Center of HPCMP and the Minnesota Supercomputing Institute.

References

Bensow, R. E. and Bark, G. "Implicit LES predictions of the cavitating flow on a propeller". Journal of Fluids Engineering, 132(4):1–10, 2010.

Colonius, T. "Modeling artificial boundary conditions for compressible flow". Annual Review of Fluid Mechanics, 36:315–345, 2004.

Coutier-Delgosha, O., Fortes-Patella, R., and Reboud, J-L. "Evaluation of the turbulence model influence on the numerical simulations of unsteady cavitation". Journal of Fluids Engineering, 125(1): 38–45, 2003.

Coutier-Delgosha, O., Stutz, B., Vabre, A., and Legoupil, S. "Analysis of cavitating flow structure by experimental and numerical investigations". Journal of Fluid Mechanics, 578:171–222, 2007.

Dittakavi, N., Chunekar, A., and Frankel, S. "Large eddy simulation of turbulent–cavitation interactions in a venturi nozzle". Journal of Fluids Engineering, 132(12):1–12, 2010.

Ganesh, H. Bubbly shock propagation as a cause of sheet to cloud transition of partial cavitation and stationary cavitation bubbles forming on a delta wing vortex. PhD thesis, University of Michigan, 2015.

Gnanaskandan, A. and Mahesh, K. "Large eddy simulation of sheet to cloud cavitation". In Proceedings of the 30th Symposium on Naval Hydrodynamics, pages 1–13, 2014.

Gnanaskandan, A. and Mahesh, K. "A numerical method to simulate turbulent cavitating flows". International Journal of Multiphase Flow, 70:22–34, 2015.

Gnanaskandan, A. and Mahesh, K. "Large eddy simulation of the transition from sheet to cloud cavitation over a wedge". International Journal of Multiphase Flow, 83:86–102, 2016a.

Gnanaskandan, A. and Mahesh, K. "Numerical investigation of near–wake characteristics of cavitating flow over a circular cylinder". Journal of Fluid Mechanics, 790, 2016b.

Goncalves, E. and Patella, R-F. "Numerical simulation of cavitating flows with homogeneous models". Computers & Fluids, 38(9):1682–1696, 2009.

Ji, B., Luo, X.W., Wu, Y., Peng, X., and Duan, Y. "Numerical analysis of unsteady cavitating turbulent flow and shedding horse–shoe vortex structure around a twisted hydrofoil". International Journal of Multiphase Flow, 51:33–43, 2013.

Ji, B., Luo, X. W., Arndt, R. E. A., Peng, X., and Wu, Y. "Large eddy simulation and theoretical investigations of the transient cavitating vortical flow structure around a NACA66 hydrofoil". International Journal of Multiphase Flow, 68:121–134, 2015.

Kim, S. "A numerical study of unsteady cavitation on a hydrofoil". In Proceedings of the 7th International Symposium on Cavitation, number 56, pages 1–13, 2009.

Koop, A. and Hoeijmakers, H. "Numerical simulation of unsteady three–dimensional sheet cavitation". In Proceedings of the 7th International Symposium on Cavitation, number 26, pages 1–12, 2009.

Laberteaux, K. R. and Ceccio, S. L. "Partial cavity flows. Part 1. Cavities forming on models without spanwise variation". Journal of Fluid Mechanics, 431:1–41, 2001.

Leroux, J-B., Astolfi, J. A., and Billard, J. Y. "An experimental study of unsteady partial cavitation". Journal of Fluids Engineering, 126(1):94–101, 2004.

Mahesh, K., Kumar, P., Gnanaskandan, A., and Nitzkorski, Z. "Les applied to ship research". Journal of Ship Research, 59(4):238–245, 2015.

Park, N. and Mahesh, K. "Numerical and modeling issues in LES of compressible turbulence on unstructured grids". In Proceedings of the 45th AIAA Aerospace Sciences Meeting and Exhibit, AIAA Paper, number 0722, pages 1–18, 2007.

Saito, Y., Takami, R., Nakamori, I., and Ikohagi, T. "Numerical analysis of unsteady behavior of cloud cavitation around a NACA0015 foil". Computational Mechanics, 40(1):85–96, 2007.

Schnerr, G. H., Sezal, I. H., and Schmidt, S. J. "Numerical investigation of three–dimensional cloud cavitation with special emphasis on collapse induced shock dynamics". Physics of Fluids, 20(4): 1–9, 2008.

Seo, J. H. and Lele, S. "Numerical investigation of cloud cavitation and cavitation noise on a hydrofoil section". In 7th International Symposium on Cavitation, number 0062, pages 1–15, 2009.

Shen, Y. and Dimotakis, P. E. "The influence of surface cavitation on hydrodynamic forces". In Proceedings of 22nd American Towing Tank Conference, pages 44–53, 1989.

Singhal, A. K., Athavale, M. M., Li, H., and Jiang, Y. "Mathematical basis and validation of the full cavitation model". Journal of Fluids Engineering, 124(3):617–624, 2002.

Spalart, P. R. and Allmaras, S. R. "A one equation turbulence model for aerodynamic flows.". AIAA Journal, 94(439):1–22, 1992.

Yee, H. C., Sandham, N. D., and Djomehri, M. J. "Low–dissipative high–order shock–capturing methods using characteristic–based filters". Journal of Computational Physics, 150(1): 199–238, 1999.